Inorganic Chemistry Communications 170 (2024) 113365

Contents lists available at ScienceDirect

Inorganic Chemistry Communications

journal homepage: www.elsevier.com/locate/inoche

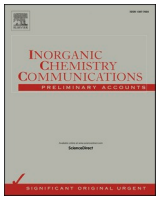

Short communication

Synergistic impacts of novel tantalum doping in $BiVO_4$ for effective photocatalytic applications, antimicrobial activity, and antioxidant aspect

Tahir Iqbal [a,*,1], Muhammad Tauseef Qureshi [b,c,**], Rabia Shahzad [a,1], Sumera Afsheen [d], Sabah Kausar [a], Ghazala Yunus [b], Muhammad Salim Mansha [a], Lubna Aamir [e], Rana Mustansar Munir [f], Hamed A. El-Serehy [g], Muhammad Yaqoob Khan [h], Basheer M. Al-Maswari [i]

[a] Department of Physics, Faculty of Science, University of Gujrat, Hafiz Hayat Campus, Gujrat 50700, Pakistan
[b] Department of Basic Sciences, College of Preparatory Year, University of Ha'il, Ha'il 55476, Saudi Arabia
[c] Department of Diagnostic Radiology, College of Applied Medical Sciences, University of Ha'il, Ha'il 2240, Saudi Arabia
[d] Department of Zoology, Faculty of Science, University of Gujrat, Hafiz Hayat Campus, Gujrat 50700, Pakistan
[e] Department of Physics, College of Science for Girls, Aja Campus, University of Ha'il, Ha'il 8145, Saudi Arabia
[f] Institute of Advanced Study, College of Physics and Optoelectronic Engineering, Shenzhen University, Shenzhen, Guangdong 518060, PR China
[g] Department of Zoology, College of Science, King Saud University, P.O. Box 2455, Riyadh 11451, Saudi Arabia
[h] Department of Physics, Kohat University of Science and Technology (KUST), Kohat 26000, Pakistan
[i] Department of Chemistry, Yuvaraja's College, University of Mysore, Manasagangotri, Mysuru 570 006, India

ARTICLE INFO

Keywords:
Co-precipitation method
Ta-doped $BiVO_4$
Tantalum
Bismuth vanadate
Photocatalytic activity
Methylene blue dye
Optical characteristics

ABSTRACT

This paper reports the production of pure and Ta-doped (1 %, 2 %, 3 %, and 4 %) $BiVO_4$ nanoparticles (NPs) for MB dye degradation. UV–Vis, FTIR, SEM, PL, and XRD techniques were used to analyze the samples. Photocatalysts ($BiVO_4$, Ta-doped $BiVO_4$) NPs have been used to study the photocatalytic activity of these materials for the degradation of methylene blue (MB) in response to visible light. The band gap reduction from 2.7 to 1.98 eV and the photogeneration of electron-hole pairs have also been demonstrated by UV–visible and PL spectroscopy. According to FTIR spectroscopy analysis, Bismuth, Tantalum, Vanadium, Oxygen, and Carbon are all present in the synthesized material. As the dopant concentration rises, the XRD data show that the crystallite size decreases. The crystallite size of the optimal (4 % Ta-doped $BiVO_4$) is 23 nm, whereas the crystallite size of the 2 % Ta-doped $BiVO_4$ is 39 nm. The SEM image shows that particle size reduces when dopant concentration rises. In comparison to previous synthesized materials, the 4 % Ta-doped $BiVO_4$ NPs have a smaller band gap, crystalline size, and recombination rate. Therefore, using the co-precipitation process, 4 % Ta-doped $BiVO_4$ NPs degrade the MB dye (86 %) in 120 min, making them an ideal material. The findings of this study will be applied to wastewater treatment.

1. Introduction

1.1. Water Pollution

The idea of life is unimaginable without water, making it a necessary resource for humans and all living things to have in its pure form. Because of its potential qualities, including its power, solubility, and other qualities, water is also referred to as a universal solvent. Water contamination is still a major global problem that can be attributed to some factors, including poor drainage, industrial waste, problems with marine dumping, and radioactive waste [1]. Watercourses have been found to include new pollutants that are not biodegradable substances that grow in the ecosystem and bioaccumulate via the food chain. They might be harmful to the environment, microbiota, and human health [2]. A major global concern that harms the water quality in water bodies is the direct disposal of wastewater into streams and rivers without

* Corresponding author.
** Corresponding author at: Department of Basic Sciences, College of Preparatory Year, University of Ha'il, Ha'il 55476, Saudi Arabia.
E-mail addresses: tahir.awan@uog.edu.pk (T. Iqbal), tauseefqureshi1981@gmail.com (M.T. Qureshi), 22011710-012@uog.edu.pk (S. Kausar).
[1] Authors contributed equally.

https://doi.org/10.1016/j.inoche.2024.113365
Received 20 June 2024; Received in revised form 14 September 2024; Accepted 17 October 2024
Available online 24 October 2024

sufficient treatment [3]. One common organic compound in water is dyes. Industrial sectors use synthetic dyes extensively; over 800,000 tonnes are produced annually worldwide [4].

1.2. Enhanced applications

Because there is little regulation or continuous regularization attempts, pharmaceutical waste is classified as an emerging contaminant. Many medications have been discovered in surface, wastewater, and groundwater over the past thirty years, including anesthesia, hormones, antibiotics, and chemotherapy agents [5]. Antibiotics such as ciprofloxacin and sulfamethoxazole are not recyclable, genetically hazardous, and have been shown to affect microorganisms in treatment plants and the microbial flora in wastewater discharge at concentrations as low as 17 μg/L [6]. Organic materials that are difficult to remove can never be fully removed by conventional waste treatment processes. For instance, following treatments with chlorination, sorption, and filtration, residual pharmaceutical concentrations have been shown to reach as much as 60 % of the baseline pharmacologic level [7]. TiO_2, ZnO, and ZnS are semiconductor photo-catalysts with high photoelectric chemistry capabilities, non-toxicity, reasonable cost, and appropriate conductivity band (CB) and valance band (VB) positions. Conventional semiconductor photocatalysts have a significant band gap, but their ability to absorb UV light is limited. This limits their potential application in the photocatalytic degradation of organic pollutants present in sewage [8]. Therefore, the main goal of safety-related research is to identify the best visible light-driven semiconductor photocatalysts [8]. Metal vanadate nanoparticles have used in photocatalysis, batteries, implantable cardiac defibrillators, and catalysis [9].

1.3. $BiVO_4$'s properties

The photocatalyst $BiVO_4$, which is powered by visible light, is increasingly important. The crystallizations of $BiVO_4$ produce three different types of crystals: tetragonal zircon (t-z), monoclinic scheelite (m-s), and tetragonal scheelite (t-s). The monoclinic scheelite phase is included into this crystalline phase. $BiVO_4$ exhibits enhanced photocatalytic activity in the presence of sunshine due to an isolated pair distortion of the Bi 6 s orbital within the semiconductor. Photogenerated carriers of charge become more portable due to the significant valence band crossover between the O 2p and Bi 6 s orbitals, which increases photocatalytic activity [10]. When exposed to visible light, monoclinic $BiVO_4$ with a moderate band gap (2.4 eV) offers the maximum photodegradation efficiency for pollutants such as organic dyes and phenolic chemicals [11]. Because of its good photocatalytic properties and narrow band gap (2.4 eV), bismuth vanadate ($BiVO_4$) is a prominent photo anode in photo electro-catalytic water treatment, attracting interest from researchers [12]. Review studies demonstrate that $BiVO_4$ is widely employed for photocatalysis in water treatment. $BiVO_4$ is mostly used for water splitting in photoelectrochemical applications [10]. An affordable, non-hazardous n-type semiconductor with remarkable chemical and photostability is bismuth vanadate ($BiVO_4$). $BiVO_4$'s photocatalytic, ferroelasticity, acoustic-optical, and ionic conductivity properties have led of many technological applications in recent years [13]. Pucherite, Clinobisvanite, and Dreyerite are the three polymorphs of $BiVO_4$ that have different crystal structures. Pucherite polymorph, the biologically produced mineral of $BiVO_4$, has an orthorhombic crystalline structure [14]. The global ecology is seriously threatened by organic pollutants, particularly color, from the leather, textile, and food industries. Organic dyes like rhodamine-B and crystal violet are commonly utilized in many different industries, but they also significantly contribute to environmental contamination [15]. Numerous approaches, such as aqueous, homogeneous precipitation, co-precipitation, solution combustion, sonochemical, hydrothermal and isothermal treatment, and reverse-micro emulsion processes, can be used to synthesize monoclinic bismuth vanadate (m-$BiVO_4$). Its visible-light photocatalytic activity is widely recognized [16]. Because of its simplicity, low cost, and scalability for large-scale production, the co-precipitation method is frequently used to synthesize $BiVO_4$ [17]. The drawbacks of this method include the requirement for several controlling factors, including high temperatures, chemical homogeneity, and particle size [18]. Finding the ideal pH to modify the crystalline electrical and morphological properties of $BiVO_4$ nanoparticles is the main objective. The basic, optical, and photocatalytic properties of $BiVO_4$ synthesized in basic media are examined in this work. Monoclinic structures of $BiVO_4$ crystallites are formed as the pH shifts from acidic to basic. The produced $BiVO_4$ nanoparticles were examined employing energy dispersive X-rays, XRD, SEM, UV–Vis Photoluminescence spectroscopy, and morphological, chemical, and optical analysis. Due to its surface Plasmon resonance (SPR) band features and synchronized oscillation of free carriers triggered by incident light, tantalum (Ta) has been identified as a special interest among various metal ion doping. These carriers act as photosensitive agents to increase the optical absorption of the M-SC composite system [19]. With a band gap of 3.9–4.0 eV and strategically placed valence and conduction bands, tantalum oxide is a good substitute material. Ta_2O_5 materials have been applied to solar cell sensitization, dye degradation, and hydrogen generation [20]. Ta has many appealing qualities, including a large dielectric constant, durability at high temperatures, increased reflectivity, capacitive qualities, and a wide spectrum gap. Medicinal fields that utilize Ta include epithelial stimulation, medication delivery, films with medicinal applications, and surgical equipment. The purpose of this study was to generate Ta-doped $BiVO_4$ NPs for catalysis through co-precipitation [21]. These newly developed synthetic nanoparticles show effective characteristics against the photocatalytic degradation of organic dyes and industrial contaminants [22]. In addition to describing these special NPs' exceptional qualities, several characterizations have been carried out, including cyclic and radical scavenger tests. Photocatalysis-induced dye degradation is generally portrayed in Fig. 1.1. A decade or so ago, research was published on the use of mixed metal vanadates in photocatalysis. A polycrystalline Fe1xBixVO$_4$ photocatalyst was successfully synthesized using a solid-state reaction technique. When photocatalysis was used to degrade MB dye on Fe_1xBixVO$_4$ in the presence of visible light, heterostructures demonstrated higher and more effective photocatalytic activity [23] (See Fig. 1.2).

2. Experimental methodology

2.1. Materials

Bismuth nitrate pentahydrate $Bi(NO_3)_3{\cdot}5H_2O$, distilled water (DI), ammonium meta vanadate NH_4VO_3, sodium hydroxide NaOH, and tantalum powder were used as raw materials and precursors in the synthesis of bismuth vanadate ($BiVO_4$) and Ta-doped $BiVO_4$

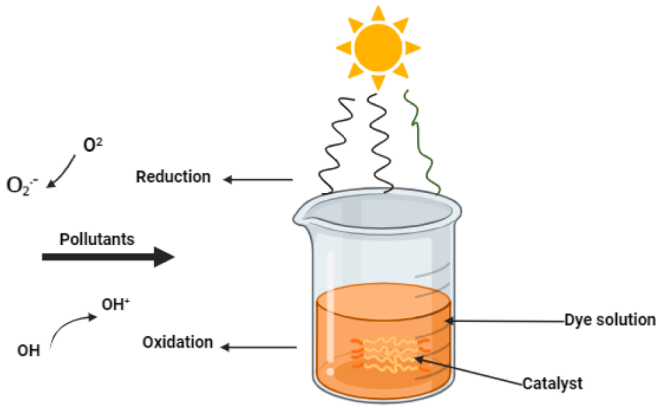

Fig. 1.1. General mechanism of photocatalysis dye degradation in catalyst.

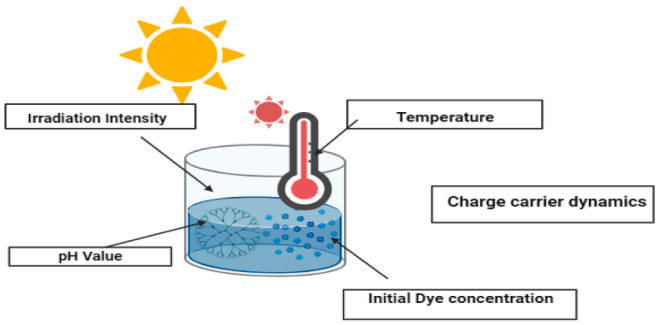

Fig. 1.2. Illustration of factors affecting photocatalysis.

nanoparticles at various percentage concentrations (1 %, 2 %, 3 %, and 4 %). The Sigma Aldrich Company provided the entire set of precursors and components needed for the current experiment.

2.2. Methodology

The co-precipitation process was utilized to create $BiVO_4$. At 70 °C, two aqueous solutions were produced. In the initial solution A, 40 ml of distilled water was used to dissolve 4 g of $Bi(NO_3)_3{\cdot}5H_2O$. For the second solution B, 1.28 of NH_4VO_3 was dissolved in 40 ml of distilled water. Solution A was added drop by drop to solution B with vigorous stirring, and then 5gm of sodium hydroxide was dissolved in 35 ml distilled water separately to increase the pH value up to 9, NaOH solution was constantly added drop by drop into the above solution with continuous stirring for 1 h, and then the tantalum precursor was added for doping purposes at different percentage concentrations (1 %, 2 %, 3 %, and 4 %), and stirred for 2 h. The pale yellowish solution was cleaned with pure ethanol and distilled water to make sure all surface-bound impurities were gone. The nanoparticles were produced after being dried for 24 h in an oven. This $BiVO_4$ powder underwent an hour-long calcination at 400 °C in a muffle furnace. Before being roughly crushed with a mortar and pestle, the material was calcined and then allowed to cool at room temperature. Lastly, 1 %, 2 %, 3 %, and 4 % Ta-doped $BiVO_4$ NPs were made (See Fig. 1.3).

2.3. Instrumental analysis

The synthesized Ta-doped $BiVO_4$ (1 %, 2 %, 3 %, and 4 %) has undergone several characterizations to examine its characteristics. A UV–visible spectrophotometer with double beam (Double Beam UV–Vis Spectrometer SP-IUV&, UOG) with a wavelength range of 200–900 nm was used to examine the optical properties as well as band gap, and photoluminescence spectroscopy (PL: RAMANLOG 6, UOG) was carried out to study the recombination rate as well as defect properties to investigate the optical properties of synthesized NPs. Unknown substances can be identified using FTIR spectra. The photocatalytic activity was used to measure the synthesized Ta- $BiVO_4$ NPs' degradation efficiency. The average particle size of nanoparticles X-ray diffraction (XRD) technique is used to study the crystal phase. An enlarged, high-resolution image can be produced with an electron microscope (SEM), and EDX analysis was used to establish the presence of NPs. Utilizing the average particle size of nanoparticles X-ray diffraction (XRD) technique, the crystal phase is examined.

3. Results and discussions

3.1. UV–Visible spectroscopy

The UV–vis spectra of pure $BiVO_4$ and Ta-doped $BiVO_4$ were examined using a UV–Vis double-beam spectrometer (Double Beam UV–Vis Spectrophotometer SP-IUV&, UOG). The photon energy is taken on the X-axis and $(ahv)^{1/2}$ on the Y-axis. The band gap value is 2.7 eV for pure and 2.5 eV, 2.3 eV, 2.2 eV, and 1.98 eV for 1 %, 2 %, 3 %, and 4 % Ta-doped $BiVO_4$ correspondingly for an indirect transition. When the Ta was added into pure $BiVO_4$ NPs at different percentage concentrations such as 1 %, 2 %, 3 %, and 4 %, and ultimately lattice the band gap decreased. Due to their lower energy values, the 4 % Ta-doped nanoparticles absorb more visible light than pure $BiVO_4$ NPs. Band gap measurements demonstrate that an increase in dopant concentration results in a decrease in the band gap, an increase in visible light absorption, and an improvement in charge carrier separation, all of which promote methylene blue photocatalytic degradation. The indirect band gap energy was calculated using the following formula.

$$(ahv)^{1/2} = C(hv - Eg) \quad (1)$$

Where c is constant, hν is incident photon energy and Eg is band gap energy (See Fig. 3.1).

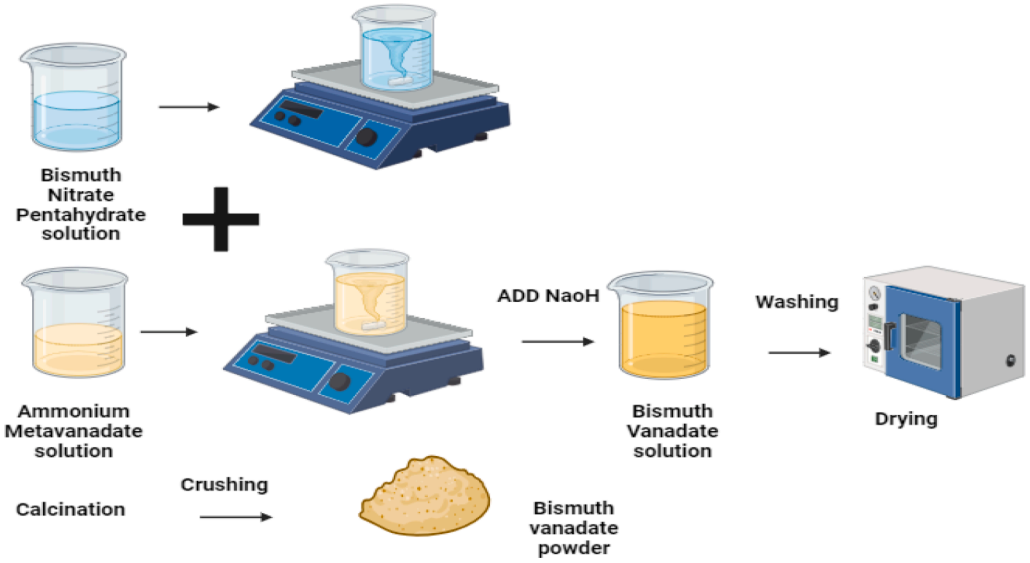

Fig. 1.3. The schematic diagram of the synthesis of $BiVO_4$ nanoparticles.

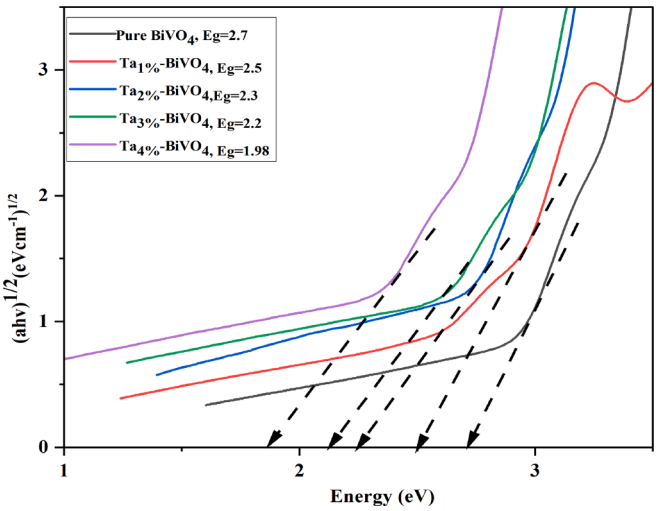

Fig. 3.1. The UV–Vis spectra of pure and Ta-doped $BiVO_4$ (1 %, 2 %, 3 %, and 4 %) NPs.

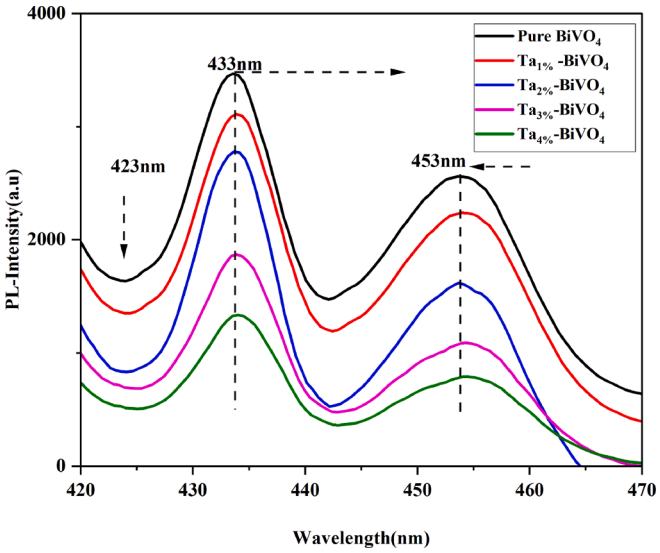

Fig. 3.2. Photoluminescence spectra of Ta-doped $BiVO_4$ with 1 %, 2 %, 3 %, and 4 % concentrations.

3.2. Photoluminescence spectroscope

Photoluminescence spectroscopy explained every flaw found in the produced nanoparticles. Photoluminescence spectroscopy is another optical characterization technique that investigates spectrum features when incoming light is diffused upon it. $BiVO_4$ nanoparticles exhibit two emission bands in the PL spectrum. Exciton collision is shown in the first band, while electron-hole pair recombination with different defects is shown in the second band. As the doping concentration rises, the peak of PL intensity falls. The $BiVO_4$ Nps doped with 4 % Ta has the lowest peak intensity, suggesting that the presence of oxygen vacancies and defects promotes recombination. Defect development and two significant excitation peaks were visible in the resulting sample's PL spectra. The excitation peak at 433 nm corresponds to the band gap peak. At 433 nm, pure $BiVO_4$ exhibits the highest intensity and recombination rate of generated charge carriers. Tantalum doping causes flaws in pure manufacturing, which lowers peak intensity and lengthens the time needed for charge carrier recombination. Peak intensity is effectively reduced by tantalum concentration. The highest dye degradation of methylene blue is created when there is a 4 % tantalum concentration because it results in the longest time delay in the recombination of generated charge carriers. Additionally, it has been found that some flaws introduced into the sample at 453 nm are responsible for the sample's dislocation development (See Fig. 3.2).

3.3. FTIR analysis

Fourier transform infrared spectroscopy was used to examine the chemical composition and the nature of the bonds. When the produced sample is exposed to infrared light, the existence of functional groups, such as stretching and bending vibrations, is detected. In FTIR spectra investigation, pure and Ta-doped $BiVO_4$ nanostructures at different concentrations (1 %, 2 %, 3 %, and 4 %) were investigated in the 500–4000 cm^{-1} range. The hydroxyl group of stretching has been found at 1435 cm^{-1}, with a larger peak due to intercalated water. Carbon with a double bond has been seen at 1982 cm^{-1}. The peak at 606 cm^{-1} and the bending at 701 cm^{-1} show the vibrational mode of Bi-O bonding, which tends to move to higher wavenumbers. Bends at 797 cm^{-1} and 854 cm^{-1} indicate V-O stretching mode. The peak at 969 cm^{-1} corresponds to Ta-O stretching mode. Wave numbers larger than 3500 cm^{-1} exhibit amazing transparency due to their low absorption nature [24] (See Fig. 3.3).

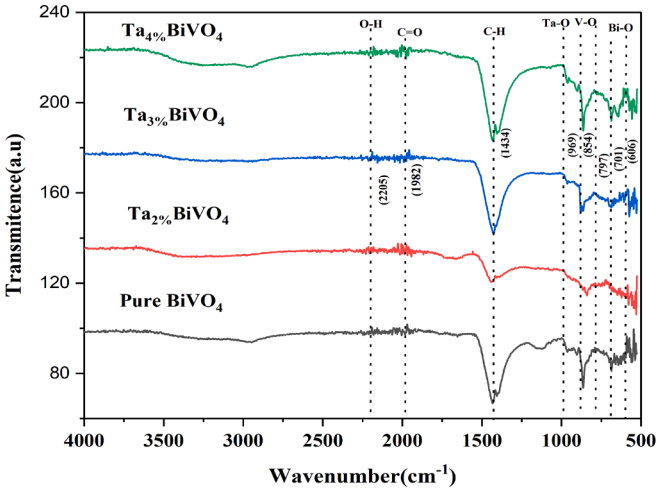

Fig. 3.3. FTIR spectra of pure $BiVO_4$ and Ta-doped $BiVO_4$ NPs (1 %, 2 %, 3 % and 4 %).

3.4. Photocatalytic activity

Photocatalytic activity is utilized to degrade organic pollutants under visible light irradiation at wavelengths greater than 420 nm. To test the degradation of MB dyes, the solution is agitated with a catalyst and then put under a xenon light. The efficiency of a degradation catalyst is determined by active surface sites, which are intimately connected to the semiconductor material's form. Other parameters affecting photocatalytic activity include temperature, pH, and catalyst loading. Under the influence of visible light, the catalyst goes through many phases to break down organic contaminants. Under the influence of visible light, the photocatalyst forms electron-hole pairs that remain in solution for a brief period. Before recombining, they react with pollutants to deteriorate. Pure $BiVO_4$ has the lowest activity rate due to its large band gap and weak absorption capabilities. The inclusion of impurity atoms is required to increase photocatalytic activity. 500 ml of distilled water was diluted with 0.01 g of MB dye for the experiment and the liquid was magnetically for 30 min in the dark. A further 0.02 g of $BiVO_4$ catalyst was added to 100 ml of MB dye solution and put in the photocatalytic reactor. For UV–vis analysis, 5 ml of prepared sample is

collected using a pipit after every 30 min. It takes 120 min to perform the whole process. The whole procedure is reported for Ta-doped $BiVO_4$ (1 %, 2 %, 3 %, & 4 %) nanoparticles and their degradation efficiency is determined by using the formula

$$\text{Efficiency of Degradation } (\%) = \left(1 - \frac{C}{C_0}\right) \times 100 \quad (2)$$

C_0 signifies the starting concentration, while C signifies the final concentration after time t. By calculating the degradation, we can deduce that the addition of Tantalum accelerates deterioration to a maximum value of 86 %. Pure $BiVO_4$ degrades less than Tantalum-doped $BiVO_4$. The 1 % Ta-doped $BiVO_4$ shows 80 % dye degradation and a rise to 4 %. The 4 % has the maximum dye degradation of 86 %. Because of its low recombination rate and vast surface area, the 4 % (optimal) tantalum-doped $BiVO_4$ exhibits the highest dye degradation of MB, as shown by UV–vis and photoluminescence studies. The electron-hole pair has the highest reduction of organic pollutants and lowers the pollutant rate from industrial waste. Absorption spectra show that dye degradation becomes minimal after 120 min of visible light irradiation with a 4 %Ta concentration, which reduces pollutants to their maximum level. The change in degradation % with Tantalum content reflects the findings of UV–vis and photoluminescence. Increasing the doping concentration reduces the recombination of produced charge carriers and increases absorption, as illustrated figure (See Fig. 3.4).

3.5. Photocatalytic degradation mechanism

Ta-doped $BiVO_4$ nanoparticles' photocatalytic degradation mechanism entails several crucial procedures that increase their effectiveness in breaking down contaminants when exposed to visible light. Ta doping increases the efficiency of charge separation and transfer inside the $BiVO_4$ structure, which accelerates the rate at which contaminants degrade [25]. Tantalum changes $BiVO_4$'s electronic structure, which encourages the formation and migration of charge carriers and, in turn, increases the material's photocatalytic activity [26]. Photo-generated electrons in the photocatalytic process are transported from the semiconductor $BiVO_4$'s valence band (VB) to its conduction band (CB) when exposed to visible light [27]. Because of the electrons being deleted during this transition, photo-generated holes are created in the VB. The electrons and holes produced by photolysis subsequently move toward the surface of the $BiVO_4$ nanoparticles [28]. Then, the photo-generated holes turn H_2O into hydroxyl radicals (•OH) while the photo-generated electrons decrease O_2 to make superoxide radicals ($O_2^{\bullet -}$). Methylene B (MB) and other contaminants can be photo-degraded by both hydroxyl and superoxide radicals. When compared to pristine $BiVO_4$, the Ta-doped $BiVO_4$ nanoparticles show better photocatalytic activity because of their increased surface area, a higher concentration of photo-generated charge carriers, and better characteristics such as oxygen vacancies that support n-type semiconductor behavior [29]. These improvements aid in the more effective breakdown of contaminants when exposed to visible light. Tantalum doping of $BiVO_4$ nanoparticles improves charge separation, increases reactive sites, and encourages the production of active species like superoxide and hydroxyl radicals, which are essential for the degradation of pollutants under visible light irradiation [30]. These factors collectively improve the photocatalytic performance of the nanoparticles. Fig. 3.5 generally describes the photocatalytic mechanism of the Ta-doped $BiVO_4$.

It is a significant requirement to explain that the UV–visible, PL, FTIR, and photocatalytic activity results that are performed by all the synthesized samples show that $Ta_{4\%}$-doped $BiVO_4$ is our efficient and optimal sample and then for budget perspective, the next characterizations such as SEM, EDX and XRD were performed of only the optimal samples.

3.6. SEM analysis

Scanning electron microscopy was used to analyze the surface of Ta-doped $BiVO_4$ samples that were made using the co-precipitation process. The shapes of pure and Ta-doped $BiVO_4$ at 2 % and 4 % were studied at various resolutions. Fig. 3.6(a) depicts the nanocluster structure with a rough surface observed in the 0.5-μm range of pure $BiVO_4$. With a 0.5-μm range at 2 %, the dendritic structure including beads was found, as depicted in Fig. 3.6(b). The morphology of the Ta-doped $BiVO_4$ sample was likewise found to be irregular, as seen in Fig. 3.6(c) and (d), with measurements made at 1 μm and 0.5 μm for 4 %, respectively. As the concentration of dopant increased, the size of the particles reduced [31].

3.7. EDX analysis

Detection of impurities using EDX was performed on samples containing 2 % and 4 % of Ta- $BiVO_4$. Energy-dispersive X-ray spectroscopy has been used to analyze the elemental composition of samples of Ta-$BiVO_4$ at 2 % and 4 %. A prominent distinctive peak containing Bismuth, Vanadium, Tantalum, Oxygen, Sodium, and Carbon has been identified in the spectra at 2 % and 4 %. The sample was handled using carbon tape, which resulted in a peak of carbon with 1.89 % weight at 2 % and 1.85 % weight at 4 % [32]. Tantalum has been successfully incorporated into Bismuth Vanadate, as seen by the notable peaks of Tantalum in 2 % and 4 %. To verify the correct distribution and composition of the materials, a quantitative analysis of the weight % data was carried out. Our samples were totally pure, with no contaminants discovered. The considerable peak of sodium is caused by the usage of sodium hydroxide to maintain pH [33].

3.8. XRD analysis

Using the X-ray diffraction method, the phase structure, composition, and crystallinity of the prepared samples have been examined. The X-ray source copper Kα has been used for the analysis of crystalline materials. The Xpert high-score software has been used for data analysis of the structures and quality of fabricated samples. To investigate the crystal structure of pure and tantalum-doped $BiVO_4$ for their use in photocatalytic processes, Tantalum is doped into bismuth vanadate by varying concentrations. The XRD pattern of pure $BiVO_4$ and Ta (1 %, 2 %, 3 % & 4 %) doped $BiVO_4$ demonstrate how pure and Ta-doped $BiVO_4$ differ from one another as shown in the figure below Fig. 3.8(a) and Fig. 3.8(b). Ta-doped $BiVO_4$ exhibits three distinct phases in the XRD diffraction pattern, which are dependent on the annealing temperature [34]. However, the material undergoes chemical dehydration and alteration upon annealing at 400 degrees Celsius, resulting in the introduction of a cubic crystal arrangement for $BiVO_4$. When the annealing temperature is raised to 500 degrees Celsius the cubic structure is transformed into a monoclinic phase for 2 % Ta-doped $BiVO_4$. This is due to the reason that the reconstructive transition is complicated by an increase of Ta ions in the $BiVO_4$ crystal lattice. The diffraction peak of pure $BiVO_4$ shows the standard cubic structure (JCPDS-card no.00-044-0429). The diffraction peak of 1 % Ta-doped $BiVO_4$ shows a monoclinic scheelite structure (JCPDS-card no.00-027-1447). The diffraction peak of 2 % Ta-doped $BiVO_4$ shows a tetragonal zircon structure (JCPDS-card no.01-073-1142), for 3 % and 4 % Ta-doped $BiVO_4$ have orthorhombic structure as according to the mentioned JCPDS numbers. Remarkably, different dopant concentrations have a prominent impact on crystal structure. This can be attributed to the structural differences between bismuth vanadate and tantalum [35]. The Scherrer formula is used to estimate the average crystalline

$$D = k\lambda/\beta\cos\theta \quad (3)$$

Where λ is the measurement of the radiation wavelength and D is the measurement of the NPs' crystallite size, β is the measurement of full-

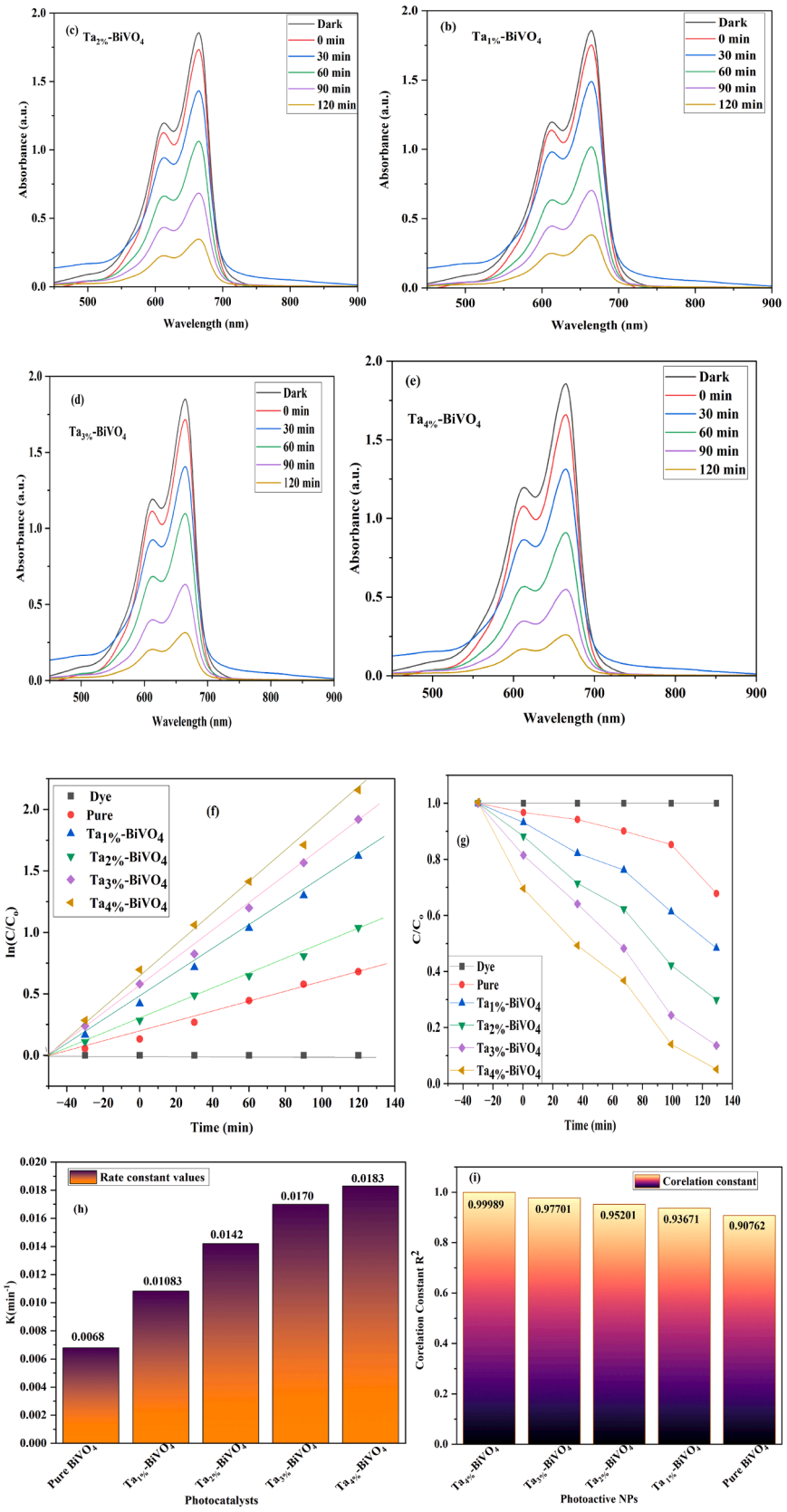

Fig. 3.4. (a) Illustrate the photocatalytic activity of pure $BiVO_4$ at 670 nm using MB dye at 120 min, and (b) illustrate the photocatalytic activity of 1 % Ta doped $BiVO_4$. (c) Illustrate the photocatalytic activity of 2 % Ta-$BiVO_4$. (d) Illustrate the photocatalytic activity of 3 % Ta-$BiVO_4$. (e) Illustrate the photocatalytic activity of 4 % Ta-$BiVO_4$. (f) Illustrate the time and $ln(C/C_o)$ for the first-order kinetics of MB dye of $BiVO_4$ and Ta-$BiVO_4$ nanoparticles (1 %, 2 %, 3 % & 4 %), (g) Illustrate the photocatalytic degradation of all the fabricated sample, figure (h) Illustrate the rate constant values, (i) depicts the correlation constant R^2 for all the fabricated samples.

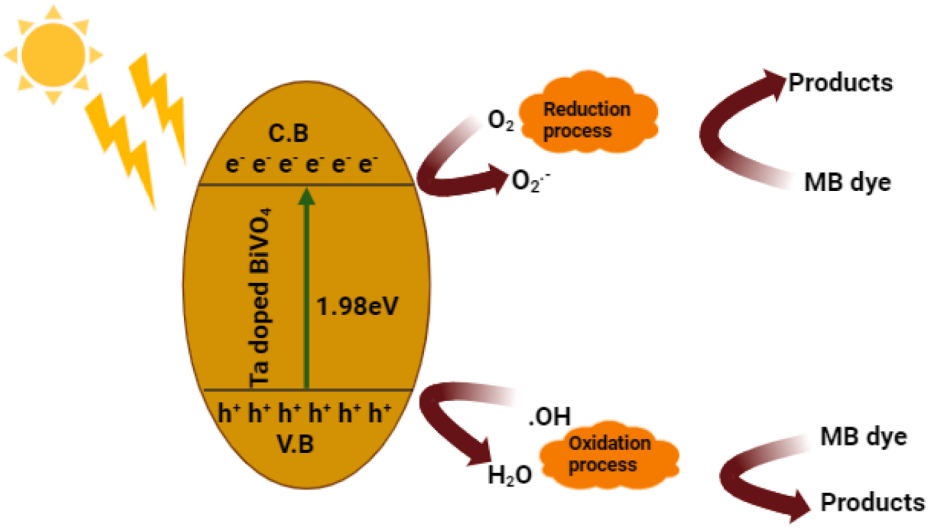

Fig. 3.5. General graphical explanation of photocatalytic degradation mechanism of methylene blue (MB) dye.

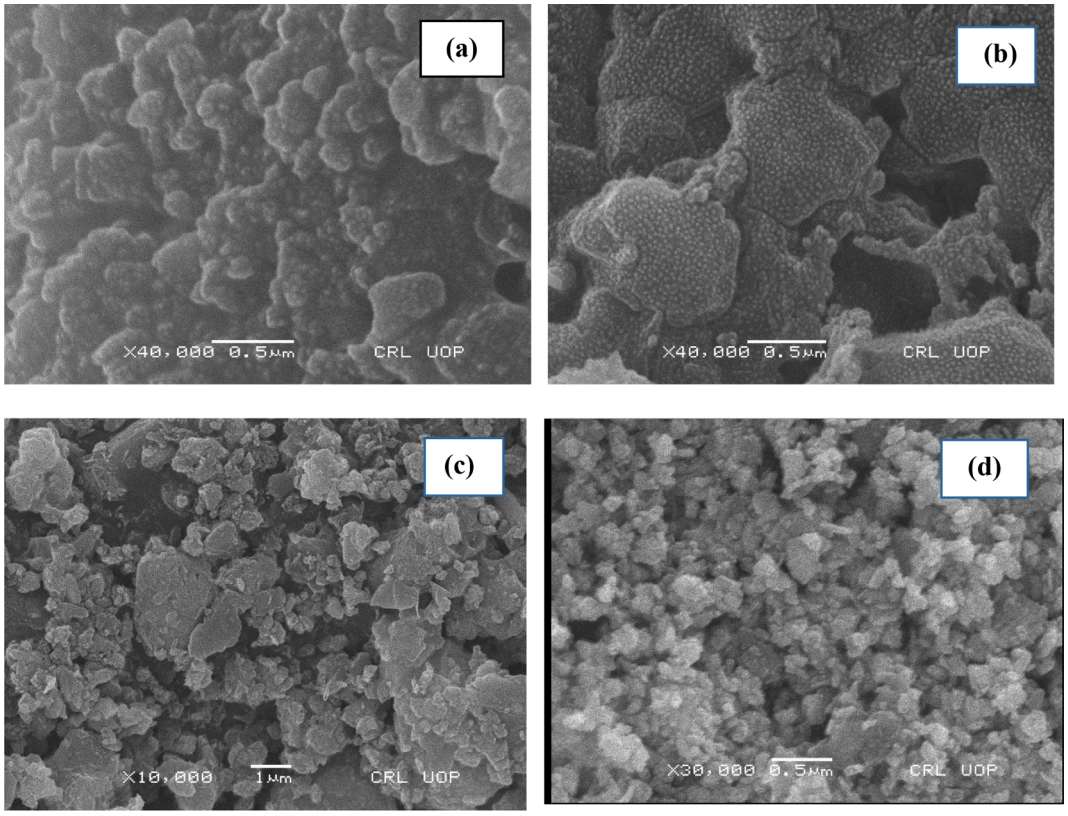

Fig. 3.6. The SEM images of (a, b) represent pure and 2 % Ta-doped $BiVO_4$ at 0.5 μm, and (c, d) represent 4 % Ta-doped $BiVO_4$ at 1 μm and 0.5 μm.

width half maximum (FWHM) in the radians, and θ represents the diffraction angles. The determined crystalline size of Pure $BiVO_4$ is 63 nm. By varying the concentration of doping the band gap decreases. The 1 % Ta-doped $BiVO_4$ has a crystallite size of 49 nm, 2 % and 3 % has crystallite sizes of 40 nm and 31 nm respectively, while 4 % Ta-doped $BiVO_4$ has a crystallite size of 23 nm (See Fig. 3.8).

3.9. Cyclic test

The cyclic test of tantalum-doped $BiVO_4$ nanoparticles (NPs) entails continually evaluating the nanoparticles to determine their reliability and efficacy over an extended period. This test is critical for determining the longevity and usefulness of tantalum-doped $BiVO_4$ NPs for various electrochemical photoelectrochemical water splitting for sewage treatment. Cyclic experiments allow investigators to study how nanoparticles perform underneath repeatedly stressful circumstances, revealing conclusions about their dependability and possibility of practical application for environmentally friendly solar water splitting technologies. The cyclic test is normally carried out by performing repeated cycles of photoelectrochemical observations on tantalum-doped $BiVO_4$ NPs. Each cycle involves lighting the nanoparticles and monitoring their photocurrent density at an applied voltage. The nanoparticles then undergo a

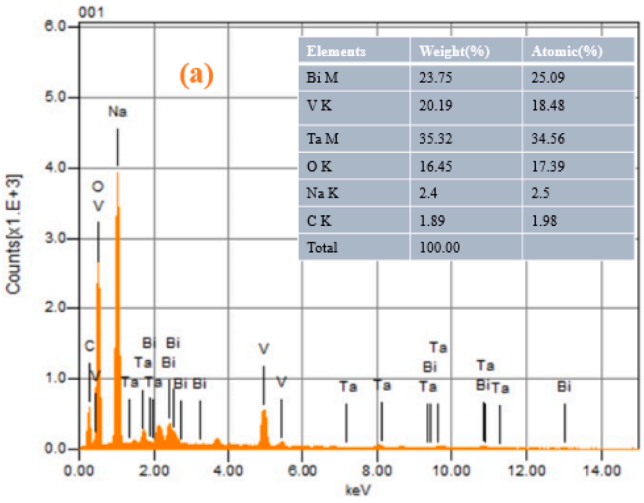

Fig. 3.7(a). The EDS spectrum of 2 % Ta-doped $BiVO_4$.

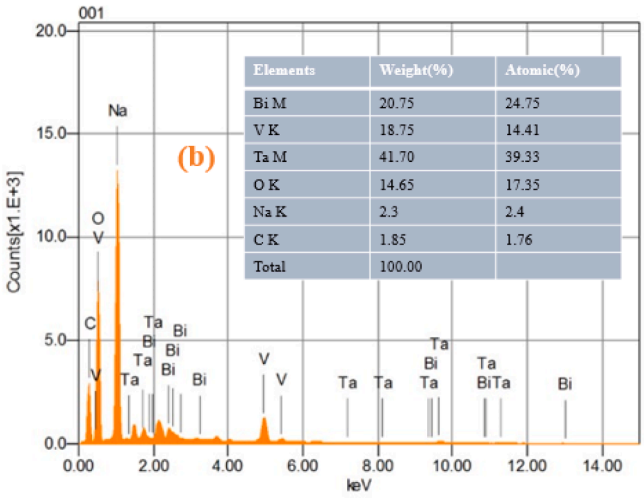

Fig. 3.7(b). The EDS spectrum of 4 % Ta-doped $BiVO_4$.

period of inactivity in the darkness before the next cycle starts. After repeating these cycles, researchers may see how the photocurrent density and other performance factors of tantalum-doped BiVO4 NPs evolve over an extended period. This understanding sheds light on the durability and endurance of the nanoparticles under working circumstances [32]. The cyclic test can help recognize any potential deterioration or impairment of performance that can happen owing to variables such as photo corrosion, surface passivation, or structural modifications in the nanoparticles. The catalyst 4 % Ta-doped $BiVO_4$ was extracted from the current study by determining its stability after usage. In the photochemical experiment, the material was repeatedly washed with acetone and water to remove any unwanted substances. It was subsequently dried at 250° for 3 h before being used in the following test. The percentage degradation of the dye resulted in just a minor loss in the photocatalytic efficacy of the catalyst after seven additional uses of 4 % Ta-doped $BiVO_4$ for MB degradation, confirming the substance's improved photocatalytic stability [36] (See Fig. 3.9).

3.10. Scavenger radical test

The scavenger test of tantalum-doped $BiVO_4$ employs H_2O_2 as an electrochemical characteristic of the photoanode. This experiment enables investigators to evaluate the effectiveness of charge transfer and recombination processes in tantalum-electrodes photoelectrodes. This test allows investigators to electrochemical behavior of tantalum-doped $BiVO_4$ both with and without the whole scavenger, offering new

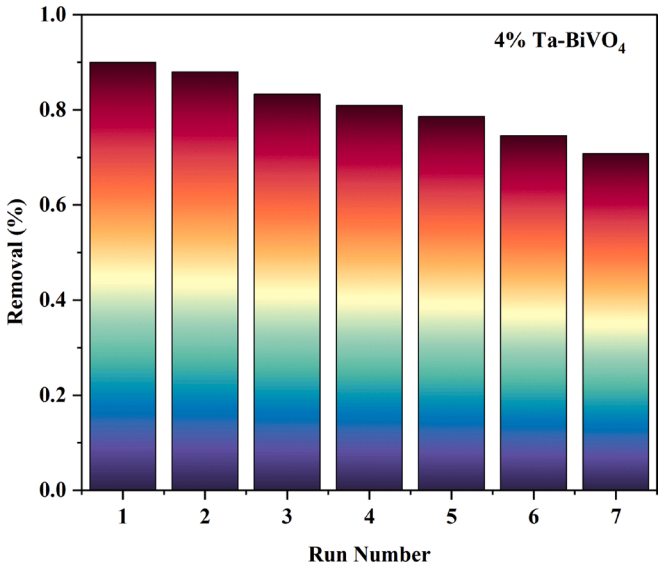

Fig. 3.9. The cyclic test of optimal sample (4 %).

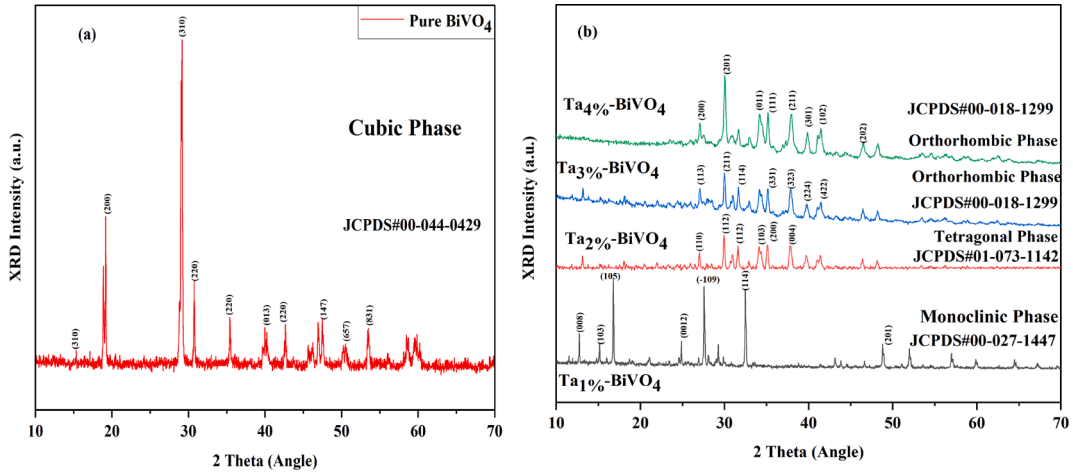

Fig. 3.8. (a) XRD analysis of pure $BiVO_4$ and (b) Ta-doped $BiVO_4$ (1 %, 2 %, 3 % & 4 %).

perspectives on the effectiveness of charge transfer and recombination mechanisms within the photoelectrodes. Tantalum-doped $BiVO_4$ photo anode had a higher photocurrent density and better charge transfer kinetics, indicating that they could be used for excellent water splitting via photoelectrochemical means [37]. By connecting the photo anode to a suitable cathode, the tantalum-doped $BiVO_4$ system might be used to produce hydrogen fuel from water splitting while also detoxifying organic contaminants in wastewater. Additionally, the capacity to modify $BiVO_4$'s operational characteristics and band structure via tantalum doping can aid electrochemical performance and photo anode stability for wastewater management operations. Tantalum-doped $BiVO_4$ can enhance charge separation and minimize surface recombination, resulting in greater solar-to-hydrogen conversion rates as well as improved elimination of pollutants [38]. Various scavengers, including Ascorbic Acid (AA), Methanol, and Isopropanol (IPA), have been shown to effectively capture superoxide radicals, holes, and hydroxyl radicals created during semiconducting material stimulation. For a better comprehension of the photocatalytic process and the role of the primary reactive elements in photocatalytic deterioration, the Figure below shows the variance in MB level as an indication of irradiation length in the presence or absence of various scavengers, including a 4 % Ta-doped $BiVO_4$ photocatalyst. Scavengers such as AA and IPA can significantly slow down the degradation rate of MB, indicating that superoxide radicals and hydroxyl radicals are the main reactive elements involved in the process of breakdown [39] (See Fig. 3.10).

3.11. Anti-oxidant properties

The antioxidant capabilities of Ta-$BiVO_4$ play a significant role in improving the photocatalytic properties of the photocatalyst. Tantalum (Ta) doping in $BiVO_4$ are enhance charge separation efficiency and reduce electron-hole recombination rates, hence improving photocatalytic performance [40].Tantalum's antioxidant capabilities explain this improvement, since they reduce oxidative species while increasing the generation of reactive oxygen species (ROS), such as hydroxyl radicals, which are required for photocatalytic degradation processes [32]. Furthermore, tantalum can be added to $BiVO_4$ to modify its surface morphology, increase its specific surface area, and promote the properties of n-type semiconductors. All of these modifications contribute to the photo catalyst's overall efficacy in breaking down organic pollutants when exposed to visible light [41].

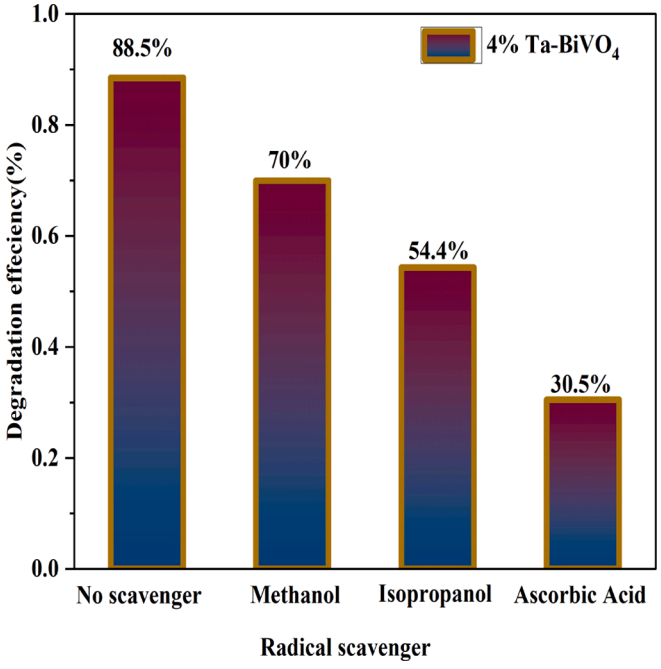

Fig. 3.10. Scavenger Radical test of 4 % Ta-$BiVO_4$.

3.12. Antimicrobial Activities

The Ta-$BiVO_4$ nanoparticles' antibacterial efficacy was assessed against two types of bacteria: Gram-positive (E. coli and Staphylococcus aureus) and Gram-negative (Escherichia coli and Pseudomonas aeruginosa). To evaluate the nanoparticles' photocatalytic antimicrobial capabilities, they were subjected to both visible light irradiation and dark ambient conditions [42]. The bacterial cultures were incubated with different doses of Ta-$BiVO_4$ nanoparticles under visible light illumination for the antibacterial assays. By measuring the zone of inhibition surrounding the areas treated with nanoparticles, the suppression of bacterial growth was tracked [43]. The findings showed that, in the absence of light, Ta-doping dramatically increased the bactericidal activity of $BiVO_4$ nanoparticles against E. coli, and S. aureus [44]. Furthermore, the bactericidal activity of the Ta-$BiVO_4$ nanoparticles was facilitated by the increased electrostatic interaction between the bacterial cell surface and the high valence of Ta^{5+}. The bacterial strains' varying cell wall composition and structure proved to be the cause of the observed variances in bactericidal efficacy.

As a result, it can be concluded that under visible light irradiation, the antimicrobial activity of Ta-$BiVO_4$ nanoparticles was successfully assessed using conventional techniques, indicating their potential as strong antimicrobial agents against both Gram-positive and Gram-negative bacteria [45]. Synthesized NPs of pure $BiVO_4$ and Ta-doped $BiVO_4$ were examined for antibacterial activity using the diffusion technique. A suitable volume of the bacterial inoculum was applied to the agar plate to inoculate the whole surface [46]. To check for contamination, the treated plates were kept at room temperature for a whole day. Discs were then put on several plates after various bacteria were infected and added to the nutrient agar. Agar with a 5 mm diameter was drilled and tagged using a stainless steel Cork borer [47]. Then, 100 μl discs and wells containing both pure and Ta-doped $BiVO_4$ NPs were introduced. Following a 24-hour incubation period at 37 °C, the antibacterial activity of Ta-doped $BiVO_4$ (4 %) and $BiVO_4$. The antibiotic ampicillin served as the control, and its zone of inhibition for E. coli and S. aureus was 8 and 9.5 mm, respectively [48]. Regarding antibacterial activity, the E. Coli bacterial strain's observed zone of inhibition was 13.5 and 16.6 mm, whereas the S. Aureus bacterial strain measured 15 and 18 mm for pure $BiVO_4$ and Ta-doped $BiVO_4$ (4 %) respectively. Fig. 3.11(a) describes that the pristine $BiVO_4$ and the 4 % Ta-doped $BiVO_4$ exhibited more potent and effective inhibitory activity against both gram-positive and gram-negative bacteria when exposed to ampicillin antibiotics.

The determined values of the zone of inhibition of pure $BiVO_4$ and Ta-doped $BiVO_4$ (4 %) for antifungal activity are 8.5 and 8 mm for the control, 12 and 11 mm for the antifungal strain of Rosellinia necatrix, and $BiVO_4$ NPs for Fusarium spp [49]. The zone of inhibition for strains of Rosellinia necatrix and Fusarium spp. is 11.5 mm and 13 mm, respectively, during the study of Ta-doped $BiVO_4$ NPs. In general, the behavior of antifungal activity is described in Fig. 3.11(b).

3.13. Graphical mechanism of antimicrobial activity

When exposed to visible light, Ta-doped $BiVO_4$ produces reactive oxygen species (ROS), which is the mechanism underlying its antibacterial action. Ta-$BiVO_4$ generates ROS, such as hydroxyl radicals (•OH), which have potent oxidative characteristics, when exposed to light [50]. By interacting with microbial cells, these ROS can cause cytoplasmic leakage, membrane permeabilization, and ultimately bacterial death. The insertion of hydrophobic groups into the bacterial membrane, which compromises its integrity and results in bacterial inactivation, is facilitated by the electrostatic contacts between the anionic lipid head groups on the surface of the bacterial membrane and the cationic

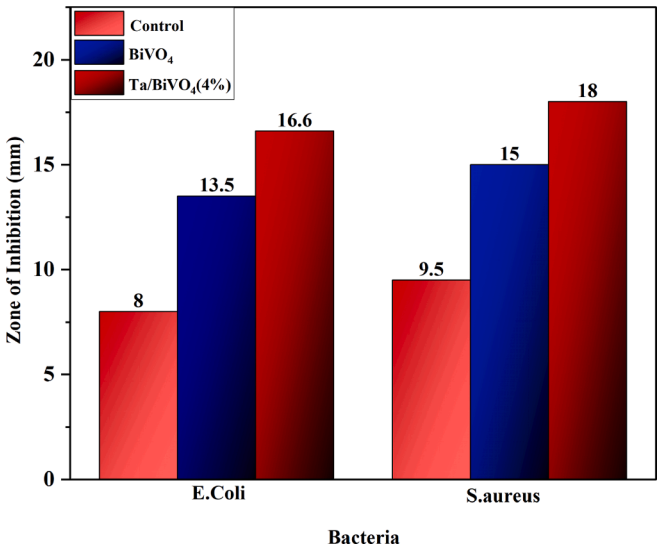

Fig. 3.11(a). Antibacterial activity of pure $BiVO_4$ and Ta-doped $BiVO_4$ (4 %).

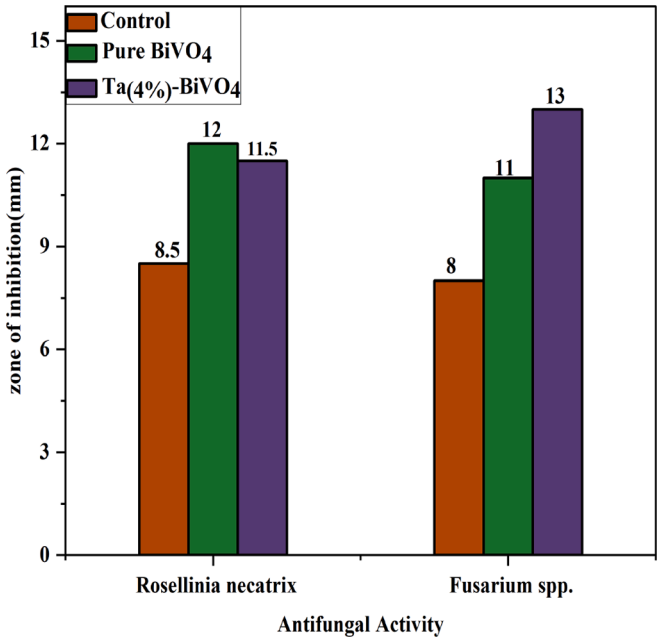

Fig. 3.11(b). Antifungal activity of pure $BiVO_4$ and Ta-doped $BiVO_4$ (4 %).

residues in the Ta-$BiVO_4$ [51]. This process demonstrates how membrane rupture and ROS production contribute to Ta-$BiVO_4$'s antibacterial activity, making it a potent photocatalyst for microbial inactivation under visible light irradiation [52]. The effects of doping with Ce and Mo on bismuth vanadate ($BiVO_4$) nanoparticles produced hydrothermally. Reactive oxygen species (ROS) may have a role in accelerating the development of resistance through DNA repair and mutagenesis, according to research on the effects of oxygen and oxidative stress on the de novo acquisition of antibiotic resistance in E. coli (See Fig. 3.12).

3.14. BET analysis

The Brunauer-Emmett-Teller (BET) Analysis has been used to determine the surface area of the prepared sample. The spectrum for the BET study is shown in Fig. 3.13. The diameter and surface area of the cavity are found to be around 1.5 nm and 45.63 m^2/g, respectively. The high surface area of dopant synthesis demonstrated the synergistic method's effect [53]. The inclusion of tantalum provides a larger surface area for redox activity when compared with pure $BiVO_4$. Finally, the improved area enhances photocatalytic and other biological uses [54].

4. Conclusion

A simple coprecipitation process has been employed for producing $BiVO_4$ and Ta-doped $BiVO_4$ NPs at various percentage concentrations (1 %, 2 %, 3 %, and 4 %), with the purpose of degrading methylene blue dye. In the coprecipitation process, 4 % Ta-doped $BiVO_4$ had the highest photocatalytic degradation efficiency. Various characterization techniques, including PL, FTIR, SEM, XRD, and UV–visible spectroscopy, show the effects of tantalum doping on $BiVO_4$ Semiconductor material. In the coprecipitation procedure, 4 % Ta doped $BiVO_4$ has the highest photocatalytic degradation efficiency of 86 % and a maximum rate constant value of 0.9999 min-1. The suppression of band gap energy from 2.7 to 1.98 eV are revealed by UV–visible spectroscopy. Up to a concentration of 4 %, the band gap is reduced and recombination decays, according to the absorption and photoluminescence measurements. Photocatalytic activity is significantly increased by increasing the doping level. When exposed to visible light for 120 min, the 4 % Ta-doped $BiVO_4$ catalyst reaches an optimised performance for MB dye degradation of 86 %. The material's purity is indicated by the EDX results. According to the SEM data, the particle size reduced as the dopant concentration increase. The SEM results show that 2 % Ta-doped $BiVO_4$ has a nanocluster form and a rough surface. For the 4 % Ta-doped $BiVO_4$ NPs, the SEM result also shows that dendritic forms containing beads are present. The synthesised compound is made of tantalum, oxygen, bismuth, and vanadium carbon, according to the FTIR spectroscopy investigation. Ta-doped $BiVO_4$ effectively produces and maintains charge carriers in the solution, resulting in higher degradation efficiency. When compared to the hydrothermal approach, the coprecipitation process is more cost effective and time efficient. Rate constants are used to rigorously calculate all of the manufactured samples, leading to the conclusion that the coprecipitation method's photocatalytic activity is superior. The efficiency of the NPs was further demonstrated by their antibacterial activity.

Ethical Approval

Not applicable.

Consent to Participate

Not applicable.

Consent to Publish

Not applicable.

Availability of data and materials

All data generated or analyzed during this study are included in this published article.

CRediT authorship contribution statement

Tahir Iqbal: Supervision, Formal analysis, Conceptualization. **Muhammad Tauseef Qureshi:** Writing – original draft, Methodology, Conceptualization. **Rabia Shahzad:** Writing – original draft, Methodology, Conceptualization. **Sumera Afsheen:** Writing – original draft, Methodology, Conceptualization. **Sabah Kausar:** Writing – original draft, Methodology, Conceptualization. **Ghazala Yunus:** Writing – original draft, Methodology, Conceptualization. **Muhammad Salim Mansha:** Writing – original draft, Methodology, Conceptualization. **Lubna Aamir:** Writing – review & editing, Validation. **Rana Mustansar**

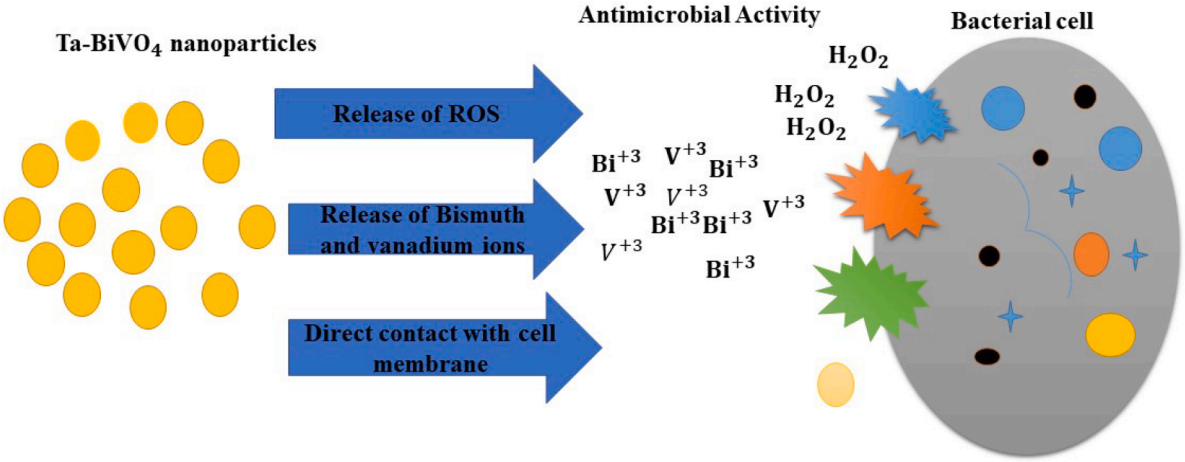

Fig. 3.12. Graphical mechanism of antimicrobial activity of pure $BiVO_4$ Ta-doped $BiVO_4$ NPs.

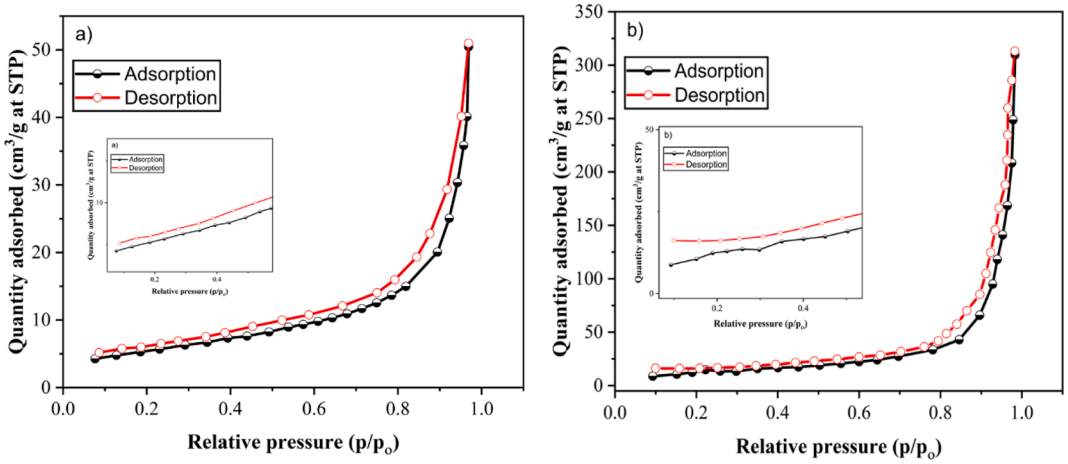

Fig. 3.13. Analysis of BET spectra.

Munir: Writing – review & editing, Validation. **Hamed A. El-Serehy:** Writing – original draft, Validation. **Muhammad Yaqoob Khan:** Writing – review & editing, Validation. **Basheer M. Al-Maswari:** Writing – review & editing, Validation.

Declaration of competing interest

The authors declare that they have no known competing financial interests or personal relationships that could have appeared to influence the work reported in this paper.

Acknowledgments

This research has been funded by Scientific Research Deanship at University of Ha'il-Saudi Arabia through project number <<RG-23 047>>.

All authors have seen and approved the final version of the manuscript being submitted. They warrant that the article is the authors' original work, hasn't received prior publication and isn't under consideration for publication elsewhere.

Data availability

Data will be made available on request.

References

[1] A. Ahmad, et al., Recent advances in new generation dye removal technologies: novel search for approaches to reprocess wastewater, RSC Adv. 5 (39) (2015) 30801–30818.
[2] G.K. Sidhu, et al., Toxicity, monitoring and biodegradation of organophosphate pesticides: a review, Crit. Rev. Environ. Sci. Technol. 49 (13) (2019) 1135–1187.
[3] S. Naidoo, A.O. Olaniran, Treated wastewater effluent as a source of microbial pollution of surface water resources, Int. J. Environ. Res. Public Health 11 (1) (2014) 249–270.
[4] M.A. Hassaan, A. El Nemr, A. Hassaan, Health and environmental impacts of dyes: mini review, Am. J. Environ. Sci. Eng. 1 (3) (2017) 64–67.
[5] J. Fick, et al., Contamination of surface, ground, and drinking water from pharmaceutical production, Environ. Toxicol. Chem. 28 (12) (2009) 2522–2527.
[6] B. Ambrosetti, L. Campanella, R. Palmisano, Degradation of antibiotics in aqueous solution by photocatalytic process: comparing the efficiency in the use of ZnO or TiO2, J. Environ. Sci. Eng. A 4 (2015) 273–281.
[7] S. Xiao, et al., Enhanced mineralization of antibiotic berberine by the photoelectrochemical process in presence of chlorides and its optimization by response surface methodology, Environ. Earth Sci. 73 (2015) 4947–4955.
[8] J. Liu, et al., Surfactants-assisted morphological regulation of BiVO4 nanostructures for photocatalytic degradation of organic pollutants in wastewater, J. Phys. Chem. Solid 172 (2023) 111079.
[9] V. Conte, B. Floris, Vanadium and molybdenum peroxides: synthesis and catalytic activity in oxidation reactions, Dalton Trans. 40 (7) (2011) 1419–1436.
[10] A. Malathi, et al., A review on BiVO4 photocatalyst: activity enhancement methods for solar photocatalytic applications, Appl. Catal. A 555 (2018) 47–74.
[11] B.-X. Lei, et al., Additive-free hydrothermal synthesis of novel bismuth vanadium oxide dendritic structures as highly efficient visible-light photocatalysts, Mater. Sci. Semicond. Process. 30 (2015) 429–434.
[12] M.M. Sajid, et al., Preparation and characterization of Vanadium pentoxide (V2O5) for photocatalytic degradation of monoazo and diazo dyes, Surf. Interfaces 19 (2020) 100502.

[13] H.L. Tan, R. Amal, Y.H. Ng, Alternative strategies in improving the photocatalytic and photoelectrochemical activities of visible light-driven BiVO 4: a review, J. Mater. Chem. A 5 (32) (2017) 16498–16521.
[14] Y. Park, K.J. McDonald, K.-S. Choi, Progress in bismuth vanadate photoanodes for use in solar water oxidation, Chem. Soc. Rev. 42 (6) (2013) 2321–2337.
[15] A. Kudo, Y. Miseki, Heterogeneous photocatalyst materials for water splitting, Chem. Soc. Rev. 38 (1) (2009) 253–278.
[16] S. Obregón, G. Colón, On the different photocatalytic performance of BiVO4 catalysts for methylene blue and rhodamine B degradation, J. Mol. Catal. A Chem. 376 (2013) 40–47.
[17] A. Martinez-de La Cruz, U.G. Perez, Photocatalytic properties of BiVO4 prepared by the co-precipitation method: degradation of rhodamine B and possible reaction mechanisms under visible irradiation, Mater. Res. Bull. 45 (2) (2010) 135–141.
[18] Y. Lu, et al., Preparation and efficient visible light-induced photocatalytic activity of m-BiVO4 with different morphologies, J. Phys. Chem. Solid 85 (2015) 44–50.
[19] R. Paul, K. Kavinarmatha, S. Parthiban, Tantalum doped titanium dioxide nanoparticles for efficient photocatalytic degradation of dyes, J. Mol. Struct. 1277 (2023) 134869.
[20] S.-Y. Wong, et al., Au nanoparticles loaded Ta2O5@ nanohoneycomb structure for visible-light-driven photocatalytic hydrogen evolution, Appl. Surf. Sci. 599 (2022) 153620.
[21] Y. Zhang, et al., Nanomaterials-enabled water and wastewater treatment, Nanoimpact 3 (2016) 22–39.
[22] Y. Rao, et al., *The effect of high temperature aging on fluorescence properties of Eu3+-doped La2 (Zr0. 7Ce0. 3) 2O7*. Ceram. Int., 50(3) (2024) 5080-5090.
[23] M.M. Sajid, et al., Experimental insights on the synthesis and characteristics of Fe1− xBixVO4 photocatalysts for efficient environmental and electrical applications, Arab. J. Chem. 16 (8) (2023) 104986.
[24] S. Muthukumaran, R. Gopalakrishnan, Structural, FTIR and photoluminescence studies of Cu doped ZnO nanopowders by co-precipitation method, Opt. Mater. 34 (11) (2012) 1946–1953.
[25] L. Liu, et al., A novel step-scheme BiVO4/Ag3VO4 photocatalyst for enhanced photocatalytic degradation activity under visible light irradiation, Chin. J. Catal. 42 (1) (2021) 46–55.
[26] S.S. Kalanur, et al., Enhanced photoactivity towards bismuth vanadate water splitting through tantalum doping: An experimental and density functional theory study, J. Colloid Interface Sci. 650 (2023) 94–104.
[27] R. Ullah, et al., Visible light photocatalytic degradation of organics on nanoparticles of bi-metallic oxides, Sep. Purif. Technol. 89 (2012) 98–106.
[28] X. Yin, et al., Boosting photoelectrochemical performance of BiVO4 through photoassisted self-reduction, ACS Appl. Energy Mater. 3 (5) (2020) 4403–4410.
[29] S. Lotfi, et al., Recent progress on the synthesis, morphology and photocatalytic dye degradation of BiVO4 photocatalysts: a review, Catal. Rev. 66 (1) (2024) 214–258.
[30] C. Lai, et al., Fabrication of CuS/BiVO4 (0 4 0) binary heterojunction photocatalysts with enhanced photocatalytic activity for Ciprofloxacin degradation and mechanism insight, Chem. Eng. J. 358 (2019) 891–902.
[31] N. Omrani, A. Nezamzadeh-Ejhieh, A comprehensive study on the enhanced photocatalytic activity of Cu2O/BiVO4/WO3 nanoparticles, J. Photochem. Photobiol. A Chem. 389 (2020) 112223.
[32] S. Ghotekar, et al., A novel eco-benevolent synthesis of BiVO4 nanoparticles using cow urine for antioxidant, anticancer, and photocatalytic activities, Biomass Convers. Biorefin. (2023) 1–17.
[33] L.E. Gomes, et al., Enhanced photocatalytic activity of BiVO4/Pt/PtOx photocatalyst: the role of Pt oxidation state, Appl. Surf. Sci. 567 (2021) 150773.
[34] C. Ma, et al., BiVO4 ternary photocatalyst co-modified with N-doped graphene nanodots and Ag nanoparticles for improved photocatalytic oxidation: a significant enhancement in photoinduced carrier separation and broad-spectrum light absorption, Sep. Purif. Technol. 264 (2021) 118423.
[35] O.A. Sánchez, et al., High performance of Ag/BiVO4 photocatalyst for 2, 4-Dichlorophenoxyacetic acid degradation under visible light, Appl. Catal. A 600 (2020) 117625.
[36] N. Omrani, A. Nezamzadeh-Ejhieh, A ternary Cu2O/BiVO4/WO3 nano-composite: Scavenging agents and the mechanism pathways in the photodegradation of sulfasalazine, J. Mol. Liq. 315 (2020) 113701.
[37] M. Ganeshbabu, et al., Synthesis and characterization of BiVO4 nanoparticles for environmental applications, RSC Adv. 10 (31) (2020) 18315–18322.
[38] N. Omrani, A. Nezamzadeh-Ejhieh, A comprehensive study on the mechanism pathways and scavenging agents in the photocatalytic activity of BiVO4/WO3 nano-composite, J. Water Process Eng. 33 (2020) 101094.
[39] K. Basavalingaiah, S. Harishkumar, G. Nagaraju, Uniform deposition of silver dots on sheet like BiVO4 nanomaterials for efficient visible light active photocatalyst towards methylene blue degradation, FlatChem 19 (2020) 100142.
[40] S. Ghotekar, et al., A novel approach towards biosynthesis of BiVO4 nanoparticles and their anticancer, antioxidant, and photocatalytic activities, J. Sol-Gel Sci. Technol. (2024) 1–11.
[41] V.G. Warrier, et al., Facile combustion synthesis of highly active Mo doped BiVO4 for photocatalytic dye degradation, photo-oxidation of alcohols, antifungal and antioxidant activities, Int. J. Environ. Anal. Chem. (2022) 1–20.
[42] M.H. de Matos Rodrigues, et al., Effect of pH on the synthesis of BiVO4 to improve photocatalysis and antimicrobial properties, Mater. Chem. Phys. 296 (2023) 127198.
[43] N. Ekthammathat, et al., Synthesis, characterization and antibacterial activity of BiVO4 microstructure, Russ. J. Phys. Chem. A 92 (2018) 1036–1040.
[44] B.G. Narváez, et al., Visible-LEDs-induced enhanced photocatalytic and antibacterial activity of BiVO4-based green photocatalysts decorated with silver and graphene, J. Photochem. Photobiol. A Chem. 447 (2024) 115191.
[45] C. Regmi, D. Dhakal, S.W. Lee, Visible-light-induced Ag/BiVO4 semiconductor with enhanced photocatalytic and antibacterial performance, Nanotechnology 29 (6) (2018) 064001.
[46] J. Ran, et al., Immobilizing CuO/BiVO4 nanocomposite on PDA-templated cotton fabric for visible light photocatalysis, antimicrobial activity and UV protection, Appl. Surf. Sci. 493 (2019) 1167–1176.
[47] H. Guan, et al., Understanding the structural-dependent photocatalytic antibacterial activity: a case study of Ag modified BiVO 4, Nanoscale Res. Lett. 15 (2020) 1–11.
[48] M. Kaur, et al., *Fabrication of magnetic heterocomposite of graphene supported CoFe2O4/BiVO4 and exploration of photocatalytic and antibacterial activities*. Mater. Today: Proc., (2023).
[49] W.A. El-Yazeed, et al., Fabrication and characterization of reduced graphene-BiVO4 nanocomposites for enhancing visible light photocatalytic and antibacterial activity, J. Photochem. Photobiol. A Chem. 417 (2021) 113362.
[50] T. Ch-Th, et al., Graphene oxide decorated TiO2 and BiVO4 nanocatalysts for enhanced visible-light-driven photocatalytic bacterial inactivation, J. Photochem. Photobiol. A Chem. 418 (2021) 113374.
[51] L. Lin, et al., Construction of Z-scheme Ag-AgBr/BiVO4/graphene aerogel with enhanced photocatalytic degradation and antibacterial activities, Colloids Surf., A Physicochem. Eng. Asp. 601 (2020) 124978.
[52] A. Nagar, S. Basu, Fabrication of carnation flower-like Bi3TaO7/Ag/BiVO4 ternary photocatalyst for boosting pollutants degradation under visible light, J. Solid State Chem. 313 (2022) 123294.
[53] X. Tao, et al., Synthesis of BiVO4 nanoflakes decorated with AuPd nanoparticles as selective oxidation photocatalysts, J. Colloid Interface Sci. 541 (2019) 300–311.
[54] R. Packiaraj, et al., Structural and electrochemical studies of Scheelite type BiVO4 nanoparticles: synthesis by simple hydrothermal method, J. Mater. Sci. Mater. Electron. 29 (15) (2018) 13265–13276.